NUCLEIC ACID THERAPEUTICS
Volume 21, Number 5, 2011

DOI: 10.1089/nat.2011.0313

Rational Truncation of an RNA Aptamer to Prostate-Specific Membrane Antigen Using Computational Structural Modeling

William M. Rockey,[1] Frank J. Hernandez,[2,*] Sheng-You Huang,[3–6,*] Song Cao,[3,4,6,*] Craig A. Howell,[2] Gregory S. Thomas,[7] Xiu Ying Liu,[2] Natalia Lapteva,[8] David M. Spencer,[8] James O. McNamara II,[2] Xiaoqin Zou,[3–6] Shi-Jie Chen,[3,4,6] and Paloma H. Giangrande[1,2,7]

RNA aptamers represent an emerging class of pharmaceuticals with great potential for targeted cancer diagnostics and therapy. Several RNA aptamers that bind cancer cell-surface antigens with high affinity and specificity have been described. However, their clinical potential has yet to be realized. A significant obstacle to the clinical adoption of RNA aptamers is the high cost of manufacturing long RNA sequences through chemical synthesis. Therapeutic aptamers are often truncated postselection by using a trial-and-error process, which is time consuming and inefficient. Here, we used a "*rational truncation*" approach guided by RNA structural prediction and protein/RNA docking algorithms that enabled us to substantially truncateA9, an RNA aptamer to prostate-specific membrane antigen (PSMA),with great potential for targeted therapeutics. This truncated PSMA aptamer (A9L; 41mer) retains binding activity, functionality, and is amenable to large-scale chemical synthesis for future clinical applications. In addition, the modeled RNA tertiary structure and protein/RNA docking predictions revealed key nucleotides within the aptamer critical for binding to PSMA and inhibiting its enzymatic activity. Finally, this work highlights the utility of existing RNA structural prediction and protein docking techniques that may be generally applicable to developing RNA aptamers optimized for therapeutic use.

Introduction

RNA aptamers are synthetic, single-stranded oligonucleotide ligands typically 30 to 70 bases in length that adopt complex 3-dimensional (3D) conformations to bind targets with high affinity and specificity (Dassie et al., 2009; Keefe et al., 2010). The targets of RNA aptamers include small molecules, peptides, proteins (secreted factors, intracellular proteins, and membrane receptors), and even whole cells (Dassie et al., 2009; Keefe et al., 2010). High-affinity RNA aptamers for specific targets can be derived from combinatorial RNA sequence libraries (with complexities of $\sim 10^{14}$) by an iterative selection process termed SELEX (Systematic Evolution of Ligands by EXponential Enrichment) (Ellington and Szostak, 1990; Jellinek et al., 1995). To enable the use of RNA aptamers for *in vivo* applications, modified nucleotides [eg, 2′-fluoropyrimidines (Ruckman et al., 1998; Biesecker et al., 1999; Rusconi et al., 2002), 2′-amino pyrimidines (Lin et al., 1994; Jellinek et al., 1995), or 2′-*O*-methyl ribose purines and pyrimidines (Burmeister et al., 2005, 2006)] are usually incorporated during the selection process or postselection during chemical synthesis (Huang et al., 1997; Padilla and Sousa, 1999).

The affinities and specificities of RNA aptamers for their targets are comparable to those of antibodies for their antigens. Similar to antibodies, RNA aptamers can be used for targeted diagnostics and therapeutics. At the bench, RNA aptamers have been successfully used as inhibitors of their targets (Thiel and Giangrande, 2009) as well as to deliver chemotherapeutic agents (Bagalkot et al., 2006; Dhar et al.,

Departments of [1]Radiation Oncology and [2]Internal Medicine, University of Iowa, Iowa City, Iowa.
Departments of [3]Physics and Astronomy and [4]Biochemistry, University of Missouri, Columbia, Missouri.
[5]Dalton Cardiovascular Research Center, University of Missouri, Columbia, Missouri.
[6]Informatics Institute, University of Missouri, Columbia, Missouri.
[7]Molecular and Cellular Biology Program, University of Iowa, Iowa City, Iowa.
[8]Department of Pathology and Immunology, Baylor College of Medicine, Houston, Texas.
*These three authors contributed equally to this work.

2008; Gu et al., 2008; Cao et al., 2009), nanoparticles (Farokhzad et al., 2004), radionuclides (Hicke et al., 2006), and siRNAs (Chu et al., 2006; McNamara et al., 2006; Zhou et al., 2008, 2009; Dassie et al., 2009; Pastor et al., 2010) to specific cell types in culture and *in vivo*. Several RNA aptamers are currently undergoing clinical trials (Biesecker et al., 1999; Dyke et al., 2006; Gilbert et al., 2007; Cosmi, 2009; Buff et al., 2010; Eikelboom et al., 2010; Mongelard and Bouvet, 2010) and one, *Pegaptanib*, was approved for therapeutic use in age-related macular degeneration by the U.S. Food and Drug Administration in 2004 (Gragoudas et al., 2004; Chakravarthy et al., 2006; Ng and Adamis, 2006). As targeted therapeutic agents, RNA aptamers have several advantages compared with antibodies, such as smaller size, better tissue penetration, ease of chemical synthesis/modification, and the lack of immune stimulation. Further, from the standpoint of pharmaceutical manufacturing, RNA aptamers are not classified as biological agents, thus easing regulatory approval.

Despite these advantages, a current obstacle to delivering RNA aptamer technology to the clinic cost effectively is the ability to chemically synthesize long RNAs (>60 nucleotides) in large-scale quantities (Reese, 2005). Aptamer production is based on solid-phase phosphoroamidite chemistry via an automated process used for small-scale oligonucleotide synthesis. This process is highly reproducible, thus allowing short synthetic RNA aptamers (15–50 nucleotides in length) to be purified to a high degree of purity/stability and synthetic yield. However, RNA aptamers of long length remain difficult to synthesize under these conditions. Although the efficiency of the manufacturing process for synthetic oligonucleotides continues to improve, perhaps the simplest way to ensure high synthetic yield is to decrease the length of the oligonucleotide sequence to be synthesized. One potential solution to this problem is the identification of shorter RNA aptamer sequences through the use of short RNA SELEX libraries (<50 nucleotides in length). However, the downside to this approach is a reduction in the sequence complexity of the overall RNA aptamer library that could compromise the identification of optimal sequences (Sassanfar and Szostak, 1993).

Several approaches have been described for reducing the length of long RNA aptamers to minimal functional sequences. These approaches often require significant experimental efforts (Burgstaller et al., 1995; Green et al., 1995; Katilius et al., 2007). Perhaps the most common method for truncating RNA aptamers postselection is a trial-and-error approach that is often time consuming and arduous. A notable example of this has been the truncation of RNA aptamers that bind to prostate-specific membrane antigen (PSMA) (Lupold et al., 2002). The trial-and-error approach was successfully used by Lupold and colleagues to truncate one of 2 nuclease-resistant RNA aptamers (A9 and A10) that had been selected to inhibit PSMA enzymatic activity (Lupold et al., 2002). By consecutively removing 5 bases from the 3′-terminus, the authors were able to truncate the A10 RNA aptamer from 71 to 56 nucleotides (A10-3) while retaining functionality (ability to inhibit PSMA enzymatic activity) and ability to be *in vitro* transcribed by using a T7 RNA polymerase. However, when a similar truncation approach was applied to the A9 aptamer in this study, the aptamer was rendered inactive.

Given the therapeutic potential of the PSMA RNA aptamers for applications including inhibition of PSMA's procarcinogenic properties (Silver et al., 1997; Lapidus et al., 2000; Colombatti et al., 2009; Yao et al., 2010) and delivery of small molecule drugs/toxins (Bagalkot et al., 2006; Dhar et al., 2008, 2011), therapeutic siRNAs (McNamara et al., 2006; Dassie et al., 2009; Pastor et al., 2010), and nanoparticles (Farokhzad et al., 2004) to prostate cancer cells, further optimization to facilitate large-scale chemical synthesis of these RNAs is compelling. Toward this end, we have employed computational RNA structural modeling and RNA/protein docking models to guide the truncation of the A9 PSMA RNA aptamer. This analysis resulted in a truncated derivative of the A9 aptamer (A9L, 41mer), which, due to its reduced length, is now amenable to large-scale chemical synthesis. Importantly, A9L retains PSMA binding activity/specificity and functionality. Specifically, we show that A9L inhibits PSMA's enzymatic activity and, when directly applied to cells expressing PSMA, is effectively internalized.

In summary, these studies demonstrate the utility of computational RNA secondary and tertiary structure models for guiding/enabling truncations of RNA aptamers while retaining their function. Further, these studies have resulted in versions of the PSMA A9 aptamer that due to their shorter sequence length are now amenable to large-scale chemical synthesis for therapeutic applications.

Materials and Methods

DNA templates and primers for generating the duplex DNA used for transcription of the RNA aptamers

A9a aptamer: DNA Template: 5′-GGGAGGACGATGCGGACCGAAAAAGACCTGACTTCTATACTAAGTCTACGTTCCCAGACGACTCCC -3′

5′ primer: 5′-TAATACGACTCACTATAGGGAGGACGATGCGGA-3′

3′ primer: 5′-GGGAGTCGTCTGGGAA-3′

A9baptamer: DNA Template: 5′-GGGACGATGCGGACCGAAAAAGACCTGACTTCTATACTAAGTCTACGTTCCCAGACGCCC-3′

5′ primer: 5′-TAATACGACTCACTATAGGGACGATGCGGACCG-3′

3′ primer: 5′-GGGCGTCTGGGAACGT-3′

A9c aptamer: DNA Template: 5′-GGGATGCGGACCGAAAAAGACCTGACTTCTATACTAAGTCTACGTTCCCAGACCC-3′

5′ primer: 5′-TAATACGACTCACTATAGGGATGCGGACCGAAA-3′

3′ primer: 5′-GGGTCTGGGAACGTAG-3′

A9daptamer: DNA Template: 5′-GGGACGATGCGGACCGAAAAAGACCTGACTTCTATACTAAGTCTACGTTCCCAGACGACCC-3′

5′ primer: 5′-TAATACGACTCACTATAGGGACGATGCGGACCG-3′

3′ primer: 5′-GGGTCGTCTGGGAACG-3′

A9eaptamer: DNA Template: 5′-GGGCGGACCGAAAAAGACCTGACTTCTATACTAAGTCTACGTTCCCACC-3′

5′ primer: 5′-TAATACGACTCACTATAGGGCGGACCGAAAAAG-3′

3′ primer: 5′-GGTGGGAACGTAGACT-3′

A9faptamer: DNA Template: 5′-GGGCGGACCGAAAAAGACCTGACTTCTATACTAAGTCTACGTTCCCAG CCC-3′

5′ primer: 5′-TAATACGACTCACTATAGGGCGGACCGAAAAAG-3′
3′ primer: 5′-GGGCTGGGAACGTAGA-3′
A9g aptamer: DNA Template: 5′-GGGACCGAAAAAGACCTGACTTCTATACTAAGTCTACGTTCCC-3′
5′ primer: 5′-TAATACGACTCACTATAGGGACCGAAAAAGACC -3′
3′ primer: 5′-GGGAACGTAGACTTAG-3′

Chemically synthesized double-stranded DNA templates used for transcription of the RNA aptamers

A9g aptamer: Sense: 5′-TAATACGACTCACTATAGGGACCGAAAAAGACCTGACTTCTATACTAAGTCTAC GTTCCC-3′
Antisense: 5′-GGGAACGTAGACTTAGTATAGAAGTCAGGTCTTTTTCGGTCCCTATAGTGA GTCGTATTA -3′

A9h aptamer: Sense: 5′-TAATACGACTCACTATAGGGGAAAAAGACCTGACTTCTATACTAAGTCTACCCC-3′
Antisense: 5′-GGGGTAGACTTAGTATAGAAGTCAGGTCTTTTTCCCCTATAGTGAGTCGTA TTA -3′

A9i aptamer: Sense: 5′-TAATACGACTCACTATAGGGCCTGACTTCTATACTAAGCCC-3′
Antisense: 5′-GGGCTTAGTATAGAAGTCAGGCCCTATAGTGAGTCGTATTA-3′

A9j aptamer: Sense: 5′-TAATACGACTCACTATAGGGACCGAAAAAGACCTAGTCTACGTTCCC-3′
Antisense: 5′-GGGAACGTAGACTAGGTCTTTTTCGGTCCCTATAGTGAGTCGTATTA-3′

A9k aptamer: Sense: 5′-TAATACGACTCACTATAGGGACCGAAAAATACGTTCCC-3′
Antisense: 5′-GGGAACGTATTTTTCGGTCCCTATAGTGAGTCGTATTA-3′

A9L aptamer: Sense: 5′-TAATACGACTCACTATAGGGCCGAAAAAGACCTGACTTCTATACTAAGTCTACG TCCC-3′
Antisense: 5′-GGGACGTAGACTTAGTATAGAAGTCAGGTCTTTTTCGGCCCTATAGTGAGT CGTATTA-3′

A9g.1 aptamer: Sense: 5′-TAATACGACTCACTATAGGGACCGAAAAAGGCCTGACTTCTATACTAAGCCTACGTTCCC-3′
Antisense: 5′-GGGAACGTAGGCTTAGTATAGAAGTCAGGCCTTTTTCGGTCCCTATAGTGAGTCGTATTA-3′

A9g.2 aptamer: Sense: 5′-TAATACGACTCACTATAGGG AC C GAAAAAGCCCTGACTTCTATACTAAGGCTAC GTT CCC-3′
Antisense: 5′-GGGAACGTAGCCTTAGTATAGAAGTCAGGGCTTTTTCGGTCCCTATAGTGAGTCGTATTA-3′

A9g.3 aptamer: Sense: 5′-TAATACGACTCACTATAGGGACCGAAAAAGACCTGACTTCTATACTAAGTCTACGGTCCC-3′
Antisense: 5′-GGGACCGTAGACTTAGTATAGAAGTCAGGTCTTTTTCGGTCCCTATAGTGAGTCGTATTA-3′

A9g.4 aptamer: Sense: 5′-TAATACGACTCACTATAGGGACCGAAAAAGACCTGACTTCTATACTAAGTCTTC GTT CCC-3′
Antisense: 5′-GGGAACGAAGACTTAGTATAGAAGTCAGGTCTTTTTCGGTCCCTATAGTGAGTCGTATTA -3′

A9g.5 aptamer: Sense: 5′-TAATACGACTCACTATAGGGACCGAAAAAGACCTGACTTCTATACTAGGTCTAC GTT CCC-3′
Antisense: 5′-GGGAACGTAGACCTAGTATAGAAGTCAGGTCTTTTTCGGTCCCTATAGTGAGTCGTATTA-3′

A9g.6 aptamer: Sense: 5′-TAATACGACTCACTATAGGGACCGAAAAAGACCTGGCTTCTATACTAAGTCTAC GTT CCC-3′
Antisense: 5′-GGGAACGTAGACTTAGTATAGAAGCCAGGTCTTTTTCGGTCCCTATAGTGAGTCGTATTA-3′

A9g.7 aptamer: Sense: 5′-TAATACGACTCACTATAGGGACCGAAAAAGACCTGACTTCTATACTAAGTCTAC GAT CCC-3′
Antisense: 5′-GGGATCGTAGACTTAGTATAGAAGTCAGGTCTTTTTCGGTCCCTATAGTGA GTCGTATTA-3′

A9g.8 aptamer: Sense: 5′-TAATACGACTCACTATAGGGACCGAAAAAGACCTGACTTCTATACTAAGTCTAC GCT CCC-3′
Antisense: 5′-GGGAGCGTAGACTTAGTATAGAAGTCAGGTCTTTTTCGGTCCCTATAGTGAGTCGTATTA-3′

RNA truncations

To generate the A9 truncations, the sequence of full-length A9 as previously reported (Lupold et al., 2002) (5′-GGGAGGACGAUGCGGACCGAAAAAGACCUGACUUCUAUACUAAGUCUACGUUCCCAGACGACUCGCCCGA-3′) was loaded into the program RNAStructure 4.6 (Mathews, 2006; Mathews et al., 2007). Using a computer-guided ''rational truncation'' approach, bases were removed from the 5′ and 3′ ends such that the predicted secondary structure of the remaining oligonucleotide was as similar as possible to that of full-length A9. Where necessary, base changes were made at the 5′ and 3′ ends to maintain a 5′-GGG transcription start codon and a complementary 3′-CCC. To create the illustrations, the secondary structures were rendered with the program VARNA 3.7 (Darty et al., 2009).

RNA transcriptions

The RNA was transcribed as previously described (McNamara et al., 2006). Briefly, template DNAs and primers were ordered from Integrated DNA Technologies (IDT). Using the primer and template sequences just described, the double-stranded DNA templates for transcription were generated as previously described (McNamara et al., 2006). DNA templates were purified with Qiagen DNA purification columns (27106) and used in *in vitro* transcription reactions as described in McNamara et al. (2006) to make individual RNA aptamers. A Y639F mutant T7 RNA polymerase (Huang et al., 1997) was used to incorporate 2′fluoro modified pyrimidines to render the RNAs resistant to nuclease degradation. The RNA from the transcription was run on a denaturing 10% acrylamide/7M urea gel, visualized using UV shadowing. The RNA was excised from the gel, eluted in 4 mL of TE buffer, washed twice with 4 mL of TE buffer, and concentrated with an Amicon 10,000 MW-cutoff spin filter (UFC801024).

As an alternative to amplifying the double-stranded DNA templates by polymerase chain reaction (PCR), the complete sense and antisense strands of the RNA transcription template were ordered from IDT. To anneal the 2, each oligonucleotide strand was added to 500 μL of PCR-grade H_2O to a final concentration of 3 μM per strand, heated to 72°C for 5 minutes, and then allowed to cool to room temperature over 10

minutes. The resulting double-stranded DNA was used in an RNA transcription reaction as just described. The aptamers A9g, A9h, A9i, A9j, A9k, A9L, and all aptamer mutations were transcribed from chemically synthesized double-stranded DNA templates in this fashion.

PSMA NAALADase activity assay

The PSMA NAALADase activity assay was modified from a previously published protocol (Xiao et al., 2000) and performed in a final reaction volume of 200 μL. Double-distilled H_2O (ddH_2O) was used in the reaction solutions. The RNA aptamers were refolded in binding buffer (20 mM HEPES, 150 mM NaCl, and 2 mM $CaCl_2$) at a concentration 1.667 times the final concentration desired in the activity assay (eg, 333 nM for a final concentration of 200 nM). Refolding was accomplished by heating at 65°C for 10 minutes, followed by cooling to 37°C for 10 minutes. A volume of 120 μL of refolded RNA in binding buffer was added to an Eppendorf tube, was combined with 40 μL of 200 mM Tris buffer, pH 7.5, and 20 μL 10 mM $CoCl_2$ (final concentrations in the reaction 40 and 1 mM, respectively). Cobalt (II) chloride was reported to be a "stimulator of enzymatic activity" in the original NAALADase assay protocol (Xiao et al., 2000). When this compound was omitted from the reaction, we observed increased nonspecific RNA interactions. Two micrograms in 2 μL of recombinant human PSMA (4234-ZN-010) from R&D Systems was diluted in 500 μL of 50 mM pH 7.5 Tris buffer. Ten microliters of the PSMA solution (40 ng PSMA) was added to the reaction mix, and the reaction was incubated for 5 minutes at 37°C to promote RNA-PSMA interaction. For the experiment shown in Fig. 1A, recombinant, purified human PSMA was obtained courtesy of Dr. David Spencer (Baylor College of Medicine). In this experiment, 2.4 μg of human recombinant PSMA protein in 10 μL of 50 mM pH 7.5 Tris buffer was added to each reaction. Ten microliters of a working solution containing 0.55 μM NAAG in H_2O having a specific activity of 10 nCi/μL of [glutamate-3,4-^{3}H]-NAAG from Perkin Elmer (NET1082250UC) was added to the reaction mixture. The reaction was allowed to proceed for 15 minutes, mixing once by pipetting at 7.5 minutes. To halt the reaction, an equal volume (200 μL) of cold 0.1 M phosphate buffer (dibasic sodium phosphate, Na_2HPO_4) was added to the reaction mixture.

AG 1-X8 formate resin (200–400 mesh) columns from Bio-Rad Laboratories (731-6221) were used to quantitate the [^{3}H]-glutamate reaction product. Before use, the columns were equilibrated with 5 mL of ddH_2O. Half of the final reaction volume (200 μL) was added to a column. The columns were eluted twice with 2 mL of 1 M formic acid. The first elution was discarded, and the second 2 mL elution was added to 10 mL of Bio-Safe II scintillation fluid (Research Products International Corp.). Activity was counted by using a Beckman-Coulter liquid scintillation counter, and was normalized to the amount of activity obtained in the reaction with no RNA added.

Filter binding assays

Filter binding assays were performed as previously described (Wong and Lohman, 1993). Briefly, aptamers were 5′-end labeled with ^{32}P by using PNK. Labeled RNAs were diluted to 2000 cpms/μL in binding buffer, heated at 95°C for 5 minutes to unfold the RNA, and allowed to refold at 37°C for 10 minutes. Five microliters of refolded labeled RNA was added to each reaction. RNA was incubated for 5 minutes with various concentrations (ranging from 1 to 1000 nM) of purified, recombinant human PSMA (4234-ZN-010) obtained from R&D Systems at 37°C. The reaction mixture was spotted onto a sandwich of nitrocellulose (Protran BA 83, 0.2 μm pore size, 10 402 488; Whatman), nylon (Zeta-Probe Blotting Membranes, 162-0153; Bio-Rad Laboratories), and Whatman 3MM chromatography paper (3130-6189) assembled in a dot-blot apparatus. Bound RNA was captured on the nitrocellulose filter, whereas unbound RNA was captured on the nylon filter. The ratio of bound:unbound RNA was calculated by exposing the filters to a storage phosphor screen and imaging with a phosphorimager.

Surface plasmon resonance (BIACore) binding measurements

Surface plasmon resonance (SPR) measurements were carried out by using a BIACore 3000 device. 5′-biotinylated RNA was generated by transcription and gel purification as just described, except that the transcription reactions were carried out in the presence of 3 mM biotin-G (Custom order from TriLink Biotechnologies: 5′-(Biotin) (Spacer 9) G-3′). The biotinylated RNA was immobilized on a streptavidin-coated Biacore chip (SensorChip SA, BR-1003-98; General Electric Company) by an injection in binding buffer at a concentration of 25 μg/mL (20 mM HEPES, pH 7.4, 150 mM NaCl, and 2 mM $CaCl_2$) at 10 μL/min. The RNA was refolded by heating to 65°C followed by cooling to 37°C before immobilization. To measure binding kinetics, 5 concentration of purified protein (prepared by serial dilutions from 250 to 15.6 nM) were injected at a flow rate of 15 μL per minute. After binding, the surface was regenerated by injecting 50 mM NaOH at a flow rate of 15 μL per minute for 20 seconds. The K_D values were calculated by global fitting of the 6 concentrations of PSMA over a constant density of A9g aptamer (1001,1 RU). The binding data were fit to a 1:1 binding with a mass transfer model to calculate kinetic parameters as previously described (Hernandez et al., 2009; Soontornworajit et al., 2011).

RNA structural modeling and PSMA docking

RNA 2-dimensional structures predictions. At the 2-dimensional (2D) structural level, an RNA structure is described by the base pairs contained in the structure. The 2D structure of an RNA is predicted from the partition function, Q, defined as the sum over all the possible conformations: $Q = \sum_s e^{-\Delta G_S/k_B T}$, where ΔG_s is the free energy of a given structure, s. The conformational sum $\sum_s$ includes all the possible secondary and pseudoknotted structures. The free energy for each given structure, ΔG_{stacks}, is determined from $\Delta G_s = \Delta G_{stacks} - T\Delta S_{loop}$, where ΔG_{stacks} is the total free energy of the base stacks as determined from the Turner rules (Serra and Turner, 1995), and $-T\Delta S_{loop}$ is the loop free energy for the secondary and pseudoknotted structures as determined from the *Vfold* model (Cao and Chen, 2005, 2006, 2009; Chen, 2008; Cao et al., 2010). To predict the 2D structures, the probability P_{ij} of finding nucleotides i and j to form a base pair is computed. P_{ij} is calculated from the conditional partition function Q_{ij}: $P_{ij} = Q_{ij}/Q$. Here, Q_{ij} is the sum over all the possible conformations containing the (i, j) base pair. From the base pairing probabilities P_{ij} for all the possible (i, j) pairs, we predict the 2D structures.

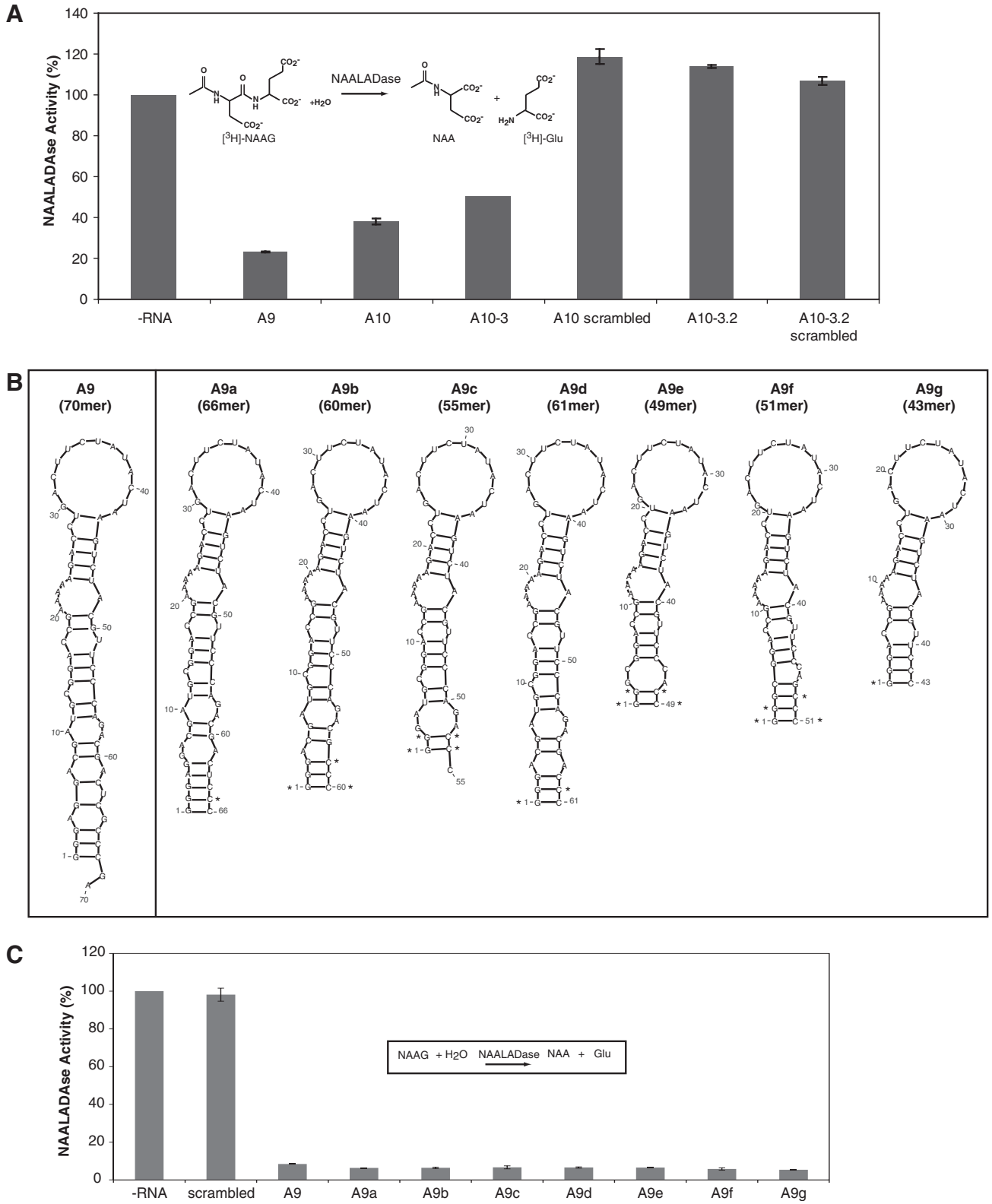

FIG. 1. Functional characterization of various truncations of the A9 PSMA RNA aptamers generated by using RNA secondary structural prediction algorithms. **(A)** RNA aptamers A9, A10, A10-3, and A10-3.2 were incubated with recombinant PSMA protein. Production of [^{3}H]-glutamate from [^{3}H]-NAAG was measured by using an NAALADase assay. RNA aptamers A10 scrambled and A10-3.2-scrambled were used as negative controls in this assay. NAALADase activity in the presence of each RNA was normalized to the no-RNA sample (−RNA). **(B)** Secondary structural predictions of truncated A9 aptamers generated using the RNAStructure 4.6 algorithm. Base changes are denoted by an asterisk (*). Base changes were introduced to retain a leading GGG transcription start codon at the 5′ end of the truncated RNA sequences or to maintain base complementarity at the 3′ end. **(C)** Effect of A9 aptamer and truncated derivatives of the A9 aptamer on PSMA enzymatic activity. NAALADase activity was normalized as in part **(A)** above. **(D)** A9 and A9g RNA aptamers inhibit PSMA NAALADase enzymatic activity with approximate IC_{50} values of 10 nM. PSMA, prostate-specific membrane antigen.

(*Figure continued*→)

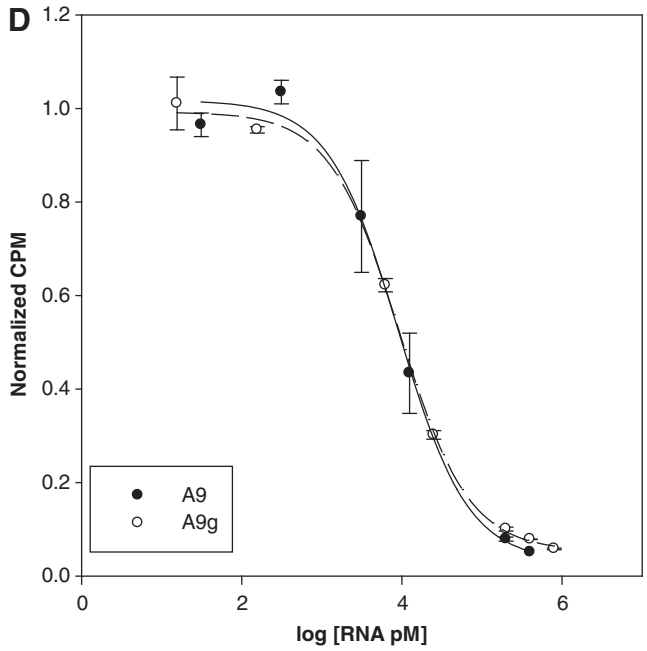

FIG. 1. (Continued).

RNA 3D structures predictions. The 3D structures of the RNAs were generated from the predicted 2D structures (Cao and Chen, 2011). The helices and loop/junctions in the structure are identified from the 2D structures. For example, the A9g structure contains 2 helices P1 and P2 and an internal loop L1, a bulge loop C16, and a hairpin loop L2. P1 is the helix from base pair G1-C43 to base pair G7-C37, and P2 is the helix from base pair A12-U35 to base pair C15-G32. The internal loop L1 includes nucleotides from A8 to A11 and nucleotide A36. The hairpin loop includes nucleotides from G18 to A30. The 3D coordinates of the helices P1 and P2 were configured by using A-form RNA helix coordinates. For the internal loop, bulge loop, and hairpin loop, the fragment-based method to search for the *optimal template structures* from the known structures in the PDB database was employed (Cao and Chen, 2011). An optimal template is defined as the template with the minimum substitution between the original loop and the template sequence. For instance, the optimal template for the internal loop L1 (5′G7AAAA3′, 5′A36C3′) was found to be the loop (5′AAAAA3′, 5′UA3′) in the PDB structure 1J5A. To achieve the optimal fit of the template structure, the terminal mismatch A11-A36 was placed within the helix P2. A 3D scaffold structure was generated based on the helices and the loop template structures. In the last step, the 3D scaffold structure was further refined by using AMBER energy minimization (Case et al., 2005).

Predicting the RNA binding modes on PSMA. The binding modes of the RNA on the PSMA were constructed by using our protein-RNA docking program. Specifically, the crystal structure of PSMA was downloaded from the Protein Data Bank (PDB code: 1Z8L) (Davis et al., 2005). Water, ions, and ligands were removed from the protein. The modeled RNA 3D structure was used for the RNA. Then, the putative binding modes of the RNA on PSMA were globally searched by using our Fast Fourier Transform-based macromolecular docking program MDockPP (Huang and Zou, 2010). MDockPP uses a hierarchical approach to construct the complexes between biological macromolecules. First, the protein was represented by a reduced model, in which each side chain on the protein surface was simplified and replaced by its center of mass. Compared with the all-atom model, the reduced model allows larger side-chain flexibility during binding mode sampling. Shape complementarity was used as a filtering criterion to generate several thousands of putative binding modes. These modes were further refined by our iteratively derived knowledge-based scoring function ITScorePP (Huang and Zou, 2008) using the all-atom model to account for the atomic details. The top-ranked binding mode that does not interfere with the putative membrane position and the PSMA dimericinterface was selected as the predicted PSMA-RNA complex.

Cell culture

The PSMA-positive prostate cancer cell line 22Rv1(1.7) was maintained as described in Dassie et al. (2009) in RPMI 1640 media with 10% FBS and 1% nonessential amino acids. The PSMA-negative prostate cancer cell line (PC3) was maintained according to the supplier's recommendations (ATCC #CRL-1435) in DMEM/F12 media with 10% FBS. Cells were maintained at 37°C with an atmosphere containing 5% CO_2.

Cell binding assay

One day before the binding assay, cells were plated in a 24-well plate at a density of ~100,000 cells per well. All subsequent procedures were performed on ice to prevent aptamer internalization. Before binding, each well was washed twice with 1 mL of ice-cold Dulbecco's phosphate-buffered saline in the absence of divalent cations (DPBS -/-) to remove growth media. Aptamers were 5′ end-labeled with ^{32}P using PNK from New England Biolabs as previously described (McNamara et al., 2008). The concentration of ^{32}P-radiolabeled aptamer was measured with UV-visible absorption spectroscopy, and serial dilutions ranging from 1000 to 0 nM were performed. To measure nonspecific binding, serial dilutions were also made containing a high fixed concentration of nonradiolabeled A9g aptamer, at 10 μM (10,000 nM). Both sets of dilutions were incubated with the cells in the 24-well plate on ice in a volume of 100 μL. After 1 hour, the binding reaction mixture was aspirated off the cells, and the cells were washed twice with 0.5 mL of ice-cold DPBS. Bound RNA was collected by washing with 0.5 mL of 0.5 N NaOH that was added to 3 mL of scintillation fluid, and activity was measured. For each dilution, specific binding was calculated by subtracting the activity of the sample with a high concentration of nonradiolabeled ("cold") aptamer added (ie, nonspecific binding) from the sample without cold aptamer added (ie, total binding). The data were plotted and fit to a one-site saturation binding model by using the nonlinear regression algorithm of the software package *Sigma Plot*. Experiments were performed in duplicate.

Cell internalization assays

22Rv1(1.7) PSMA-positive prostate cancer cells (target) and PC-3 PSMA-negative prostate cancer cells (nontarget) were grown to confluency in a 6-well plate. Cells were washed

twice with 1 mL of DPBS prewarmed at 37°C. Cells were then blocked with 1 mL of 100 μg/mL yeast tRNA prewarmed at 37°C. After 15 minutes, the block was removed, and 100 pmol RNA aptamer in DPBS was added to cells for 30 minutes at 37°C with 5% CO_2. Cells were washed once with ice-cold DPBS followed by 2 washes of ice-cold 0.5M NaCl in DPBS. The internalized RNA was recovered by using TRIzol reagent. Quantitative reverse transcription (RT)-PCR was performed by using the iScript One-Step RT-PCR Kit with SYBR Green (Cat# 170-8893) from Bio-Rad Laboratories. Samples were normalized to an internal RNA reference control. Specifically, 0.5 pmol/sample m12-23 aptamer (McNamara et al., 2008) was added to each sample along with TRIzol as a reference control. Primer sets included the internal reference primer set for m12-23 (Sel1), the A9g primer set (amplifies A9, A9g, and A9g.6), the A10 primer set (amplifies A10 and A10-3.2), and the A10-3.2 scrambled primer set. Samples were first normalized to the internal reference RNA (m12-23) and then according to the relative amount of RNA internalized vs. the nontarget control cells (PC3).

Primer sequences for the quantitative RT-PCR are as follows: Sel1 5′ primer: 5′-GGGGGAATTCTAATACGACT CACTATAGG GAGAGAGGAAGAGGGATGGG-3′; Sel1 3′ primer 5′-GGGGGGATCCAGTACTATCGACCTCT GGGTT ATG-3′; A9g 5′ primer: 5′-TAATACGACTCACTATAGGGA CCGAAAAAGACC-3′; A9g 3′ primer:5′-GGGAACGTAGA CTTAG-3′; A10 5′ primer: 5′-TAATACGACTCACTATAGG GAGGA CGATGCGG-3′; A10-3.2 3′ primer: 5′-AGGAGTG ACGTAAACATG -3′; A10-3.2 scrambled 5′ primer: 5′-TAAT ACGACTCACTATAGGGGCATGCCTAGCT-3′; A10-3.2 scrambled 3′ primer: 5′-CCGCGCATAAGCCATGGG-3′.

Results

Rational truncation of A9 PSMA RNA aptamer

The PSMA RNA aptamers A9 and A10 have been selected for their ability to inhibit PSMA's enzymatic activity (Lupold et al., 2002). Since PSMA's enzymatic activity has been implicated in carcinogenesis (metastatic potential) (Lapidus et al., 2000), optimized, truncated versions of these inhibitors promise to be valuable agents not only for targeted imaging and therapy of prostate cancer but also to directly inhibit PSMA's pro-metastatic functions. We used the NAALADase assay to assess the inhibitory activity of previously described, truncated versions of the A10 RNA aptamer: A10-3 (56 mer) (Lupold et al., 2002) and A10-3.2 (39 mer) (Fig. 1A). The NAALADase activity of PSMA hydrolyzes *N*-acetylaspartylglutamate (NAAG) to *N*-acetylaspartate and glutamate (Fig. 1A; insert). As previously described (Lupold et al., 2002), A10-3 retains NAALADase inhibitory activity, albeit less efficiently compared with the full-length A10 and A9 RNA aptamers. In contrast, A10-3.2 (39 mer) had no NAALADase inhibitory activity. This was confirmed at higher RNA concentrations up to 3.8 μM (data not shown). Scrambled versions of the A10 and A10-3.2 aptamers were used as negative controls in this assay. These scrambled aptamers have the same number of nucleotides and base composition as their wild-type counterparts but possess a "scrambled" sequence.

As previously described, A9 is a better inhibitor of PSMA enzymatic activity compared with A10 (Lupold et al., 2002). Thus, we set out to determine the NAALADase inhibitory activity of various truncations of the A9 aptamer. Previous attempts at truncating the A9 aptamer have proved unsuccessful (Lupold et al., 2002). Thus, rather than performing a series of base deletions from the 3′ end, we reasoned that maintaining the overall structure of the PSMA-interacting region of the aptamer would be essential for retaining activity. To this end, a series of 5′ and 3′-end base deletions were made, and the RNA secondary-structure prediction program RNAStructure 4.6 was used to select those truncations that retained the predicted secondary structural motifs of the full-length A9 aptamer (Fig. 1B). In addition, selective base changes were made at the 5′ and 3′ ends to maintain aT7 transcription start-site (5′GGG) and maintain base-paring complementarity at the 3′ end.

Seven initial truncated versions of the A9 aptamer were designed (A9a through A9g) with lengths ranging from 66 bases (A9a) to 43 bases (A9g). The NAALADase assay was used to assess inhibition of PSMA enzymatic activity by the various truncations. A scrambled RNA aptamer sequence (71 mer) did not inhibit enzymatic activity. Remarkably, all 7 truncations inhibited PSMA NAALADase activity as well as full-length A9 under these assay conditions (800 nM RNA) (Fig. 1C). We next determined the inhibitory potency of the shortest truncation, A9g (43 mer) compared with the full-length A9aptamer. Inhibition was tested over a range of RNA concentrations (20 pM to 800 nM). Both A9g (43 mer) and A9 (70 mer) inhibited NAALADase activity with an IC_{50} of 10 nM under the assay conditions (Fig. 1D), thus suggesting that A9g, similar to A9, retains key structural/sequence elements important for inhibition of PSMA enzymatic activity.

A second series of truncations were made in an attempt to further decrease the length of the A9g aptamer and to assess structural and sequence elements important for PSMA inhibition (Fig. 2A). The truncations A9h (37 mer) and A9i (24 mer) retain sequence and structural loop elements of A9g, whereas A9j (30 mer) and A9k (21 mer) retain sequence and structural stem elements of A9g (Fig. 2A). Interestingly, unlike A9 and A9g, none of these additional truncations (A9h-A9k) exhibited inhibitory activity under the assay conditions (200 nM RNA concentration) (Fig. 2B). Together, these results suggest that key sequence and/or structural elements for PSMA inhibition are present within bases 1–43 of the A9g aptamer.

A9g binds to PSMA with high affinity and specificity

The NAALADase activity assay provides an indirect measurement of the interaction of the PSMA aptamers with PSMA. To determine the binding profile of the A9g aptamer for PSMA, we performed filter-binding assays (Fig. 3A) and (SPR/BIACore) with recombinant, purified human PSMA protein (Fig. 3B). As determined by the filter binding assay, the A9g aptamer retains the same binding profile as the full-length A9 (Fig. 3A). A more extensive measure of binding by analyzing kinetic interaction data using SPR/BIACore was also performed. In these experiments, biotinylated A9g RNA was immobilized on streptavidin-coated gold chips. A solution containing the analyte of interest (recombinant purified PSMA protein) was injected over the chip during an association phase, thus allowing for measurement of the binding on-rate (k_{on}). After the injection was halted, the rate of

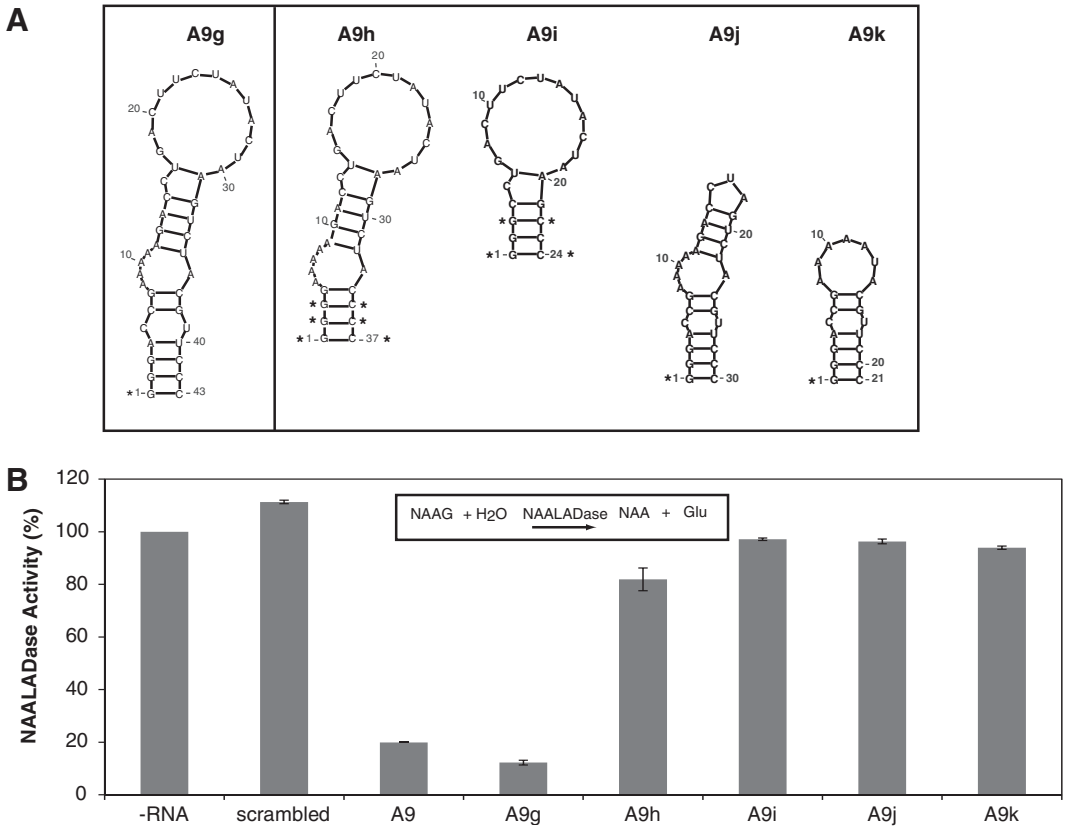

FIG. 2. Further truncation of the A9 aptamer causes loss of inhibitory activity. **(A)** Secondary structural predictions of truncated A9 aptamers generated using the RNAStructure 4.6 algorithm. Base changes are denoted by an asterisk (*). Base changes were introduced to retain a leading GGG transcription start codon at the 5′ end of the truncated RNA sequences or to maintain base complementarity at the 3′ end. **(B)** Effect of A9 aptamer and truncated derivatives of the A9 aptamer on PSMA enzymatic activity. NAALADase activity was normalized as in Fig. 1.

dissociation (k_{off}) was measured. By repeating these measurements at various analyte (PSMA) concentrations, an accurate estimation of binding was determined ($K_D = k_{off}/k_{on}$). The K_D of A9g for PSMA ranged from 5 nM to 30 nM in triplicate experiments (lowest value shown) (Fig. 3B). The differences in the absolute K_D values obtained by filter binding and SPR are likely due to the intrinsic differences with regard to these assays (Arraiano et al., 2008).

Structure-function analysis of A9g binding to PSMA

A series of base changes were introduced within A9g in an attempt to identify the sequence/structural elements necessary for binding to PSMA. Inherent in these experiments is the assumption that the base changes only create local changes in the RNA structure and not a global change in folding. For these experiments, the A9g aptamer was divided into 2 stem regions (S1 and S2) and 3 loop regions (L1, L2 and L3) (Fig. 4A). Base changes were made to either preserve or disrupt these various structural elements. The RNA-secondary structure prediction algorithm, RNAStructure 4.6, was used to predict folding of the modified A9g RNAs (A9g.1-A9g.6).

To address the importance of the S2 stem sequence, the A-U base pair in the stem region S2 was replaced with either a G-C or a C-G base pair (A9g.1 and A9g.2 respectively) (Fig. 4A). A9g.1 and A9g.2 were predicted to retain the overall secondary structure as A9g (Fig. 4A). As predicted, A9g.1 and A9g.2 resulted in RNA aptamers with comparable inhibitory activity as A9g (Fig. 4B). In contrast, a base change within S2 that was predicted to lengthen the stem (A9g.5) resulted in a loss of PSMA inhibitory activity, thus suggesting that the overall structural and not sequence elements of S2 are important for the RNA's inhibitory function. We next addressed the importance of each loop (L1, L2, and L3) by introducing base changes that would disrupt the predicted folding of the loops (A9g.3, A9g.4, and A9g.6 respectively). With the exception of A9g.4, all base changes completely abrogated the ability of the RNA aptamers to inhibit PSMA enzymatic activity (Fig. 4B), thus suggesting that the loops are required for function. In the case of A9g.4, inhibitory activity was decreased by ~50% compared with A9g. Interestingly, 2 distinct secondary structures (A9g.4a and A9g.4b) with similar minimum free energies (ΔGs) were predicted for A9g.4 (Fig. 4A). The predicted free energies of these 2 structures were -9.9 and $-9.4\,\text{kcal}\cdot\text{mol}^{-1}$, respectively. To assess whether loss of inhibitory function correlates with loss of binding to PSMA, we performed filter binding assays to determine binding of A9g.3-A9g.6 to recombinant PSMA (Fig. 4C). With the exception of A9g.4, the binding capacity (B_{max}) of PSMA for these mutants was severely diminished. The binding of A9g.4 mirrored its inhibitory activity (Fig. 4B), with a binding capacity for PSMA of ~50% compared with A9g.

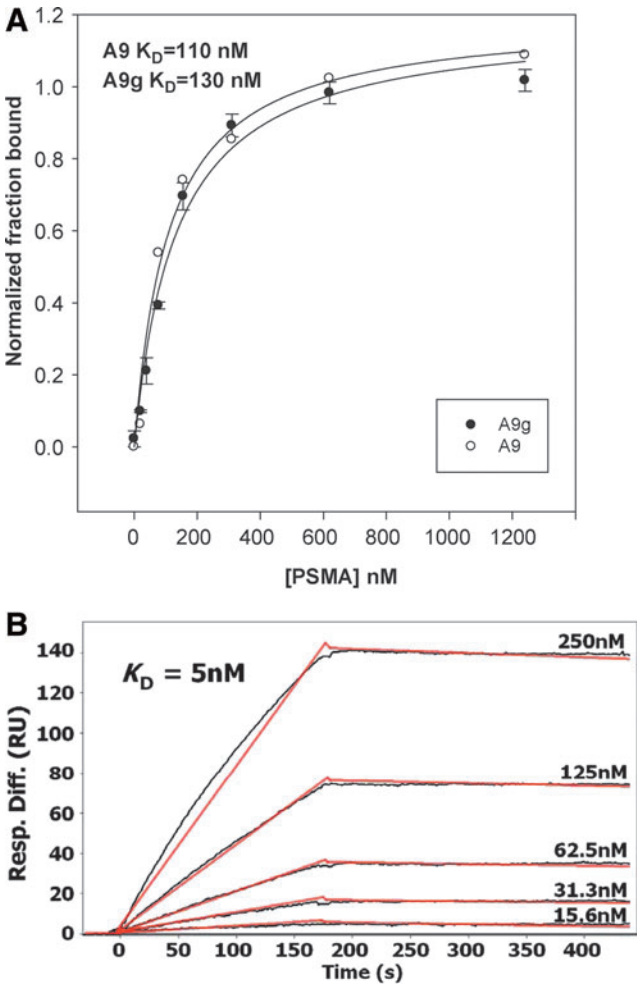

FIG. 3. Binding of A9 and A9g to human PSMA. **(A)** A saturation filter binding assay was used to measure binding of A9 and A9g to recombinant human PSMA protein. The calculated $_{KD}$ for A9 was 110 nM, and the $_{KD}$ for A9g was 130 nM. The fraction bound was normalized to the $_{Bmax}$ (maximal binding capacity) of A9. **(B)** Measurement of the binding affinity of A9g for recombinant human PSMA protein by surface plasmon resonance (SPR, BIACore). The data were fit to a 1:1 binding with a mass transfer model. The $_{KD}$ of A9g calculated from the model was 5 nM with an χ^2 value of 1.51. The on-rate (k_a) was 1.15×10^4 $M^{-1}\cdot s^{-1}$, and the off-rate ($_{kd}$) was 5.7×10^{-5} seconds^{-1}.

Assessment of binding specificity of A9g to PSMA

Binding specificity of the A9g aptamer for PSMA was determined by using SPR/BIACore (Fig. 4D; left panel). Binding specificity was assessed by comparing the k_{on} and k_{off} rates of A9g for recombinant PSMA protein (target) to the K_{on} and k_{off} rates of A9g for nontarget proteins (BSA and HER2). For these experiments, biotinylated A9g RNA was immobilized on streptavidin-coated gold chips. No appreciable interaction between A9g and the nontarget proteins (BSA and HER2) was measured (Fig. 4D; left panel). Lack of binding of A9g.6 to PSMA was also confirmed with SPR/BIACore (Fig. 4D; right panel). In addition, there was no measurable binding of A9g.6 to the nontarget proteins (BSA and HER2). These data provide confirmation of binding specificity of A9g for PSMA (Fig. 4D).

RNA tertiary structure predictions and RNA-protein docking studies

With the exceptions of A9g.1 and A9g.2 that were designed to have the same secondary structure as wild-type A9g, all the other A9g-derivatives experienced a significant decrease in their ability to inhibit and bind PSMA. It may be that each of the predicted secondary structural elements examined play a role in the aptamer's binding to PSMA. Alternatively, any of the changes made to the predicted structural elements may disrupt the "global" folding of the RNA, thus rendering it inactive.

To provide additional insight into the interaction of the A9g RNA aptamer with PSMA, a tertiary structure model of A9g was created. The predicted tertiary structure of A9g was computationally docked to a crystal structure of PSMA (Davis et al., 2005) (Fig. 5A; left panel). Interestingly, the RNA-protein docking analysis revealed 2 bases, adenosine at position 9 (A9) and uridine at position 39 (U39), that were predicted to interact directly with PSMA. The amine group of A9 forms a hydrogen bond with a backbone carbonyl of PSMA, and U39 forms multiple close van der Waals interactions with PSMA side chains. On the basis of these predictions, base changes were made to retain the hydrogen bond at position A9 (Fig. 5A; compare middle and right panels) and to test the necessity of U at position 39. Specifically, the uridine at position 39 was replaced with either an adenosine (A9g.7; U39A) or a cytosine (A9g.8; U39C), and the adenosine at position 9 was replaced with a cytosine (A9g.9; A9C) (Fig. 5A; right panel). Predicted secondary structures for these A9g variants are shown in Fig. 5B. Not surprisingly, the A9g (A9C) variant retained PSMA inhibitory activity, albeit less effectively compared with A9g (Fig. 5B). In contrast, the A9g (U39A), A9g (U39C), and A9g (U39G) variants completely lost inhibitory activity (Fig. 5B). Notably, unlike the A9g (U39G) variant (identical to A9g.3, Fig. 4A), theA9g (U39A) and A9g (U39C) variants were not predicted to alter the secondary structure of A9g (Fig. 5B). These data suggest that sequence conservation (uridine) at position 39 may be more important than the overall structure of the L1 loop for conferring the RNA aptamer's inhibitory function.

Based on the data just provided, we hypothesized that a further truncation of A9g which retains suridine at position 39 should result in an RNA aptamer with comparable PSMA inhibitory activity to A9g. To test this hypothesis, we removed the most distal G-C base-pair of A9g (A9L; 41 mer). We also introduced a base change at the first position to maintain the 5′-GGG T7 RNA polymerase transcription start (Fig. 5C; left panel). As predicted, A9L was equally as effective as A9g at inhibiting PSMA enzymatic activity (Fig. 5C; right panel). Elimination of additional bases from the 5′ or 3′ termini (eg, A9h; 37 mer) abrogated inhibition of PSMA enzymatic activity (Fig. 5C; right panel). These findings were consistent with altered folding of these shorter RNAs as predicted by using the RNA secondary structure prediction algorithm (RNAStructure 4.6) and loss of sequence elements (eg, U at position 39) required for function.

A9g and A9L bind to and internalize into PSMA-positive prostate cancer cells

Binding of A9g to PSMA expressed on the surface of prostate cancer cells was confirmed by incubating varying amounts of ^{32}P-labeled A9g with either PSMA-positive

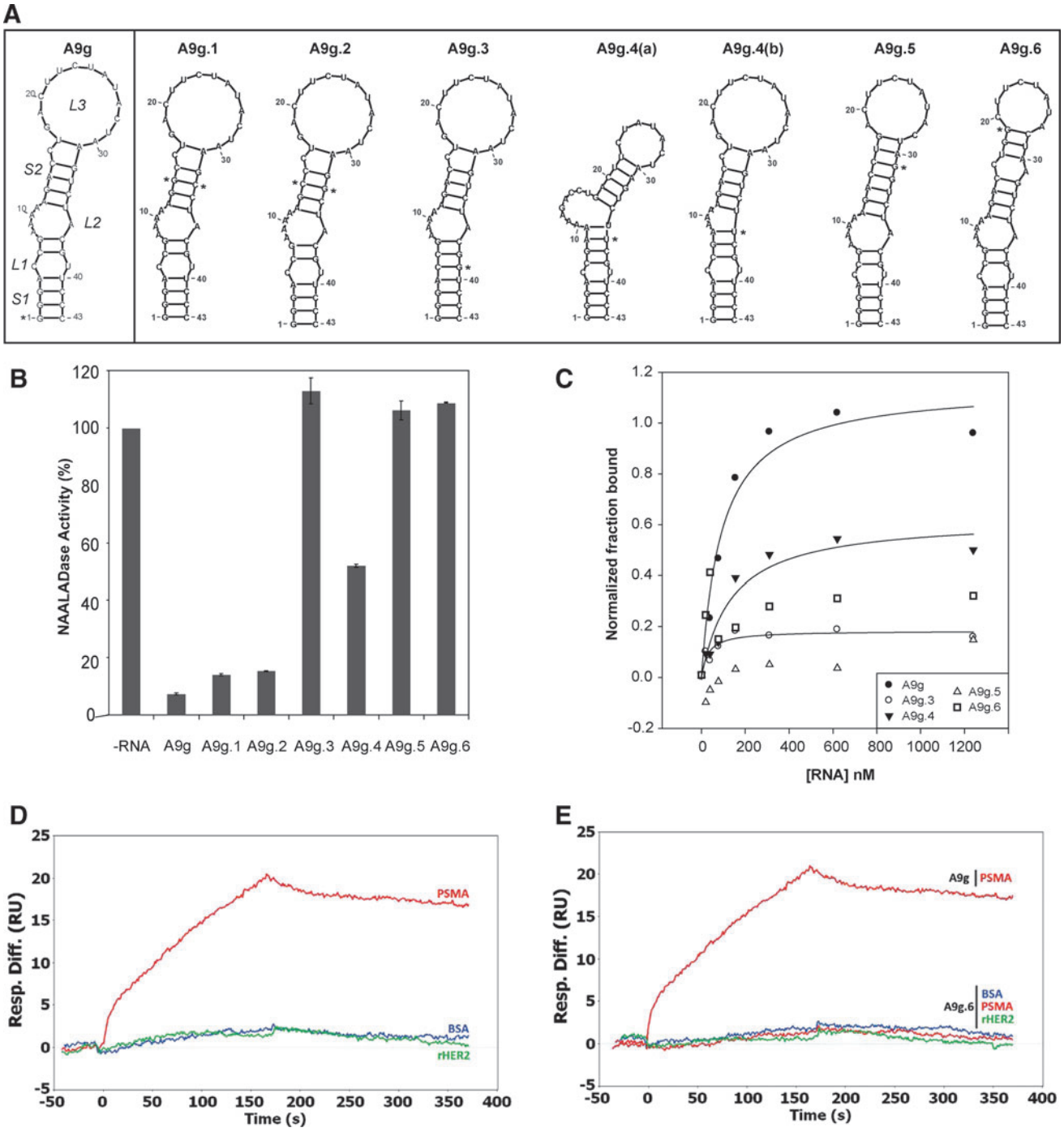

FIG. 4. Characterization of A9g binding to PSMA. **(A)** Secondary structural predictions of truncated A9 aptamers generated using the RNAStructure 4.6 algorithm. Base changes are denoted by an asterisk (*). Base changes were introduced in an attempt to either retain the predicted secondary structure (A9g.1 and A9g.2) or disrupt various secondary structural elements (A9g.3-A9g.6) of A9g. Two secondary structure predictions were given for the A9g.4 sequence, denoted by A9g.4a and A9g.4b. **(B)** Effect of A9g aptamer derivatives (A9g.1 through A9g.6) on PSMA NAALADase inhibitor activity. NAALADase activity was measured and normalized as in Fig. 1. **(C)** Saturation filter binding assay of A9g aptamer and A9g aptamer derivatives (A9g.3-A9g.6). **(D)** Binding of A9g to recombinant human PSMA, recombinant rat HER2 (rHER2), and BSA using BIACore (left panel). **(E)** Binding of A9g.6 to recombinant human PSMA, recombinant rat HER2 (rHER2), and BSA using BIACore (right panel).

(22Rv1 clone 1.7) (Dassie et al., 2009) or PSMA-negative (PC-3) prostate cancer cells on ice (to prevent internalization into the cells) (Supplementary Fig. S1; Supplementary Data are available online at www.liebertonline.com/nat). The PSMA-expressing cells were found to have a higher binding capacity for A9g compared with the PSMA-negative cells (Supplementary Fig. S1). The background binding to PC-3 cells is thought to be a result of free ^{32}P after exo-nuclease digestion on the cell surface (data not shown).

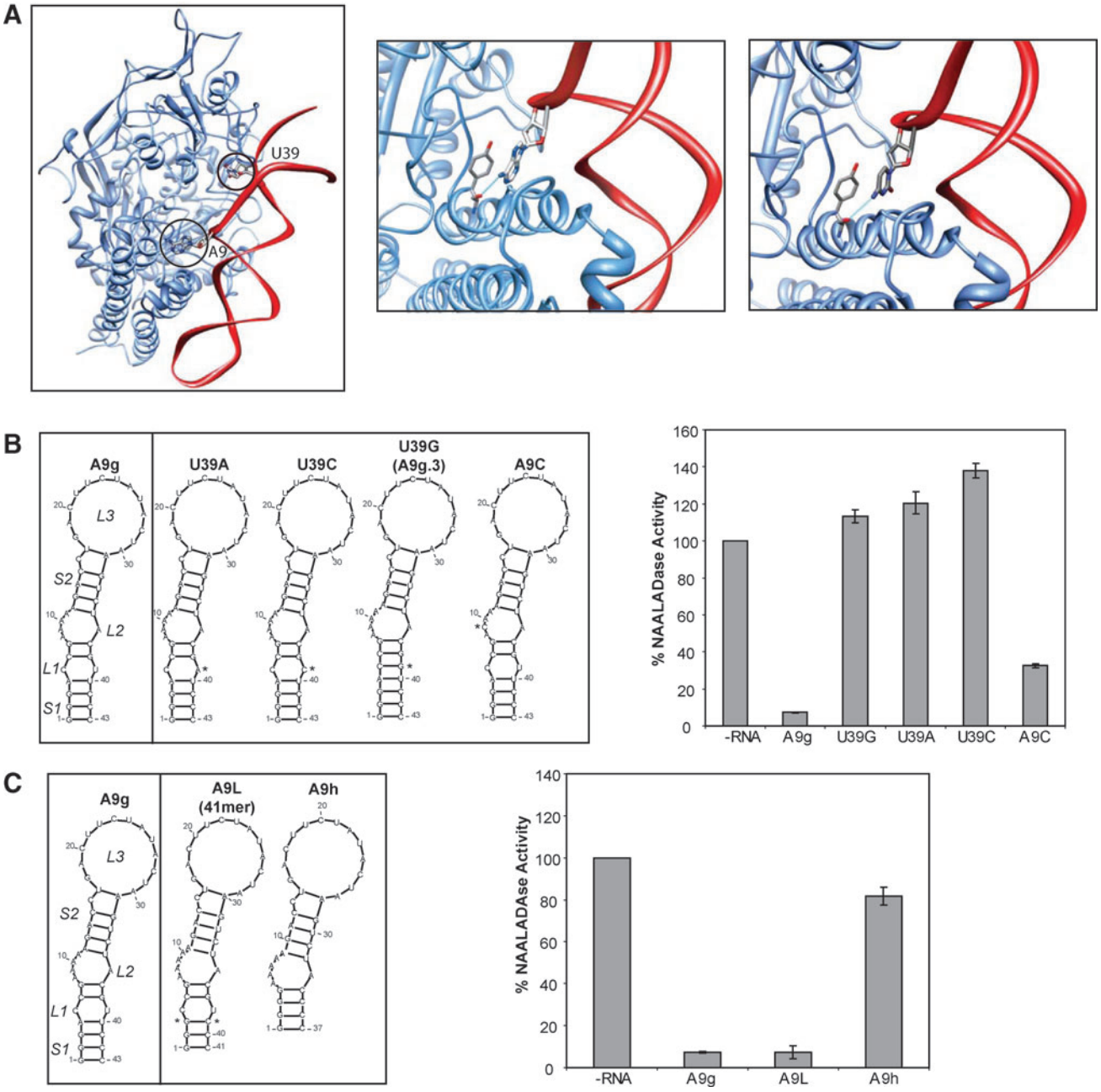

FIG. 5. Truncated A9 PSMA aptamers derived based on RNA tertiary structure and protein/RNA docking predictions. **(A)** Modeled tertiary structure of A9g docked to a crystal structure of PSMA. The bases A9 and U39 are predicted to form direct interactions with the crystal structure of PSMA. The amine group of A9 is predicted to form a hydrogen bond with a backbone carbonyl of PSMA (close up; middle panel). Right panel; close up of A9g (A9C) variant where the A at position 9 was changed to a C to retain the hydrogen bond. **(B)** Secondary structural predictions of A9g aptamer and A9g aptamer derivatives generated using the RNAStructure 4.6 algorithm (left panel). Base changes are denoted by an asterisk (*). Secondary structural predictions of A9g were generated to test the importance of the uracil at position 39 and the adenosine at position 9. Effect of A9g and A9g aptamer derivatives (U39A, U39C, U39G, and A9C) on PSMA NAALADase activity (right panel). **(C)** Secondary structural predictions of A9g aptamer and truncated derivatives A9L (41 mer) and A9h (37 mer) using the RNAStructure 4.6 algorithm (left panel). Base changes are denoted by an asterisk (*). Effect of A9L (41 mer) and A9h (37 mer) aptamers on PSMA NAALADase activity. NAALADase activity was measured and normalized as in Fig. 1 (right panel).

Aptamers that bind to cell-surface proteins (eg, cancer epitopes) can be developed for imaging applications (Hicke et al., 2006). In addition, aptamers with cell-internalizing properties can be harnessed for delivery of therapeutic agents into target cells (Bagalkot et al., 2006; Dhar et al., 2008; Gu et al., 2008; Cao et al., 2009). Both the A9 and A10 RNA aptamers were demonstrated to be effective at delivering cargos that require internalization, such as cytotoxic drugs (Farokhzad et al., 2004) and siRNAs (Chu et al., 2006; McNamara et al., 2006). For therapeutic development, the A10 aptamer

was further truncated to 39 bases (A10-3.2) while retaining the ability to bind to PSMA on the surface of cells and deliver its therapeutic siRNA cargo into PSMA-expressing prostate cancer cells (Dassie et al., 2009). Unfortunately, the shorter A10-3.2 aptamer no longer exhibits PSMA inhibitory activity (Fig. 1A). Since inhibitory activity, binding, and internalization ability do not necessarily coincide, we performed an internalization assay to assess whether the shorter A9 aptamer variants (A9g and A9L), which retain PSMA inhibitory activity (Fig. 5C), internalize into PSMA-expressing prostate cancer cells (Fig. 6A). Full-length A9, A9g (43 mer), and A9L (41mer) aptamers were incubated with either PSMA-positive (22Rv1 clone 1.7) or PSMA-negative (PC-3) prostate cancer cells at 37°C to enable cell internalization. Cells were washed with a high-salt wash buffer containing 0.5 M NaCl to remove nonbinders or aptamers bound to the surface of the cells. Internalized aptamers were recovered by Trizol extraction. The efficiency of internalization for each RNA aptamer was assessed by using quantitative RT-PCR (Fig. 6). No loss in internalization ability was observed for the truncated A9 variants (A9g and A9L) compared with the full-length A9 RNA aptamer (Fig. 6A). As expected, A9g and A9L retained specificity for cells expressing PSMA (Fig. 6A). Importantly, A9g and A9L internalized more efficiently into PSMA expressing prostate cancer cells compared with A10 and the A10 truncated variants (A10-3 and A10-3.2) (Fig. 6B). No internalization was observed with a scrambled A10-3.2 aptamer sequence or with a functionally inactive mutant of A9g (A9g.6) (Fig. 6). All A10 and A9 RNA aptamer derivatives retained specificity for PSMA expressing cells (22Rv1 clone 1.7) compared with PSMA-negative cells (PC-3) (Fig. 6B). The fold increase of RNA recovered from PSMA-expressing cells versus RNA recovered from PC-3 cells is shown for each RNA aptamer. No statistically significant difference in internalization is observed for A10 and A10-3.2 ($P = 0.1$). In contrast, the truncated A9 variants (A9g and A9L) internalized more efficiently into PSMA-expressing cells compared with either the full-length A9 aptamer ($P < 0.1$) or A10 aptamers. This could be a result of steric hindrance or interaction of a part of the aptamer with other cellular factors that may hinder or retard uptake (data not shown). Together, these data confirm that the truncated A9 aptamer variants (A9g and A9L) retain target-specific cell internalizing properties and can, thus, be developed into effective targeted delivery agents for prostate cancer.

Discussion

Here, we describe a "rational truncation" approach that takes advantage of computer-generated RNA structure models to facilitate the truncation of RNA aptamer sequences postselection. This approach enabled us to engineer truncated versions of the PSMA A9 aptamer (Lupold et al., 2002) that retain binding affinity, specificity, and functionality. Computer-generated RNA secondary structure models were used to remove bases from both the 5′- and 3′- termini of the RNA and introduce base changes to conserve those secondary structural elements that are predicted to be necessary for binding to PSMA. This analysis resulted in a 27-base truncation of the PSMA A9 RNA aptamer, yielding an RNA oligonucleotide of 43 nucleotides in length (A9g), which binds to recombinant PSMA with nanomolar affinity ($K_D = 5$ nM) (Fig. 3B) and retains PSMA inhibitory activity (Fig. 1D). Importantly, we show that similar to A9, A9g retains the ability to internalize into PSMA-expressing prostate cancer cells (Fig. 6) and, thus, could be used for targeted delivery of therapeutic agents (toxins, siRNAs, and radionuclides). In addition to computer-generated RNA secondary structure models, we

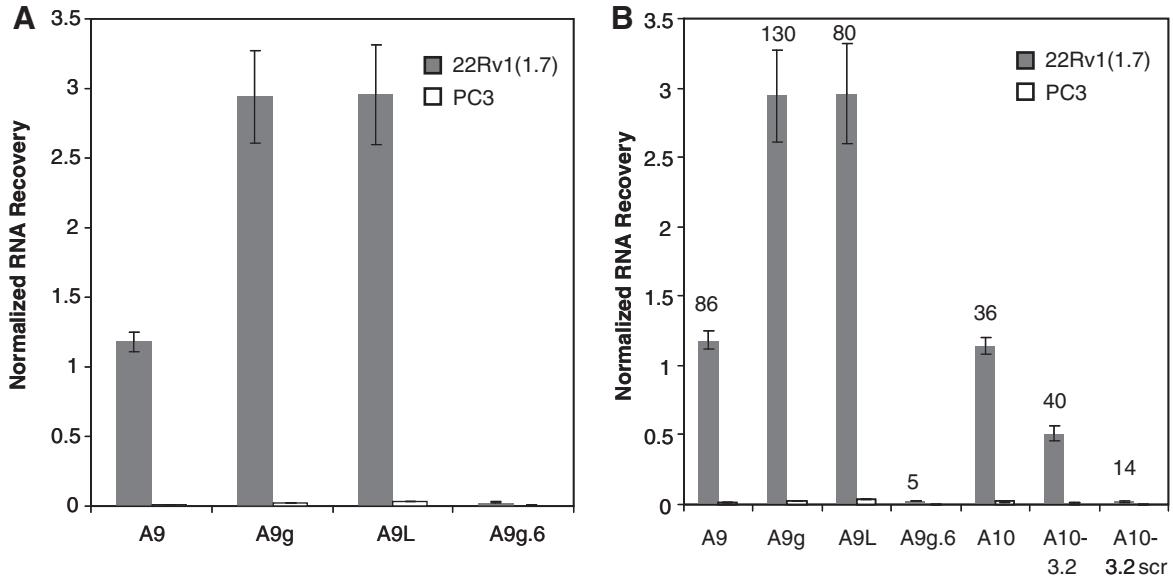

FIG. 6. Truncated A9 aptamers bind to and internalize into PSMA expressing cells. **(A)** Internalization of PSMA RNA aptamers A9, A9g (43 mer), A9L (41 mer), and A9g.6 into prostate cancer cells expressing PSMA. Internalization was measured by using quantitative reverse transcription-polymerase chain reaction. RNA recovery was normalized to recovery of an internal RNA control. **(B)** Internalization of PSMA RNA aptamers A10, A9, and derivatives into PSMA expressing prostate cancer cells. A10-3.2 scrambled and A9g.6 aptamers were used as negative controls for internalization in this assay. The fold enrichment in recovery with regard to non-PSMA expressing cells is reported.

combined predictive RNA tertiary structure models with protein docking studies to obtain further insights into the A9g-PSMA interaction (Fig. 5). This analysis revealed key nucleotides within A9g critical for binding to PSMA (Fig. 5A). Further, this analysis enabled us to perform an additional 2-nucleotide truncation of A9g, thus resulting in a 41-nucleotide-long RNA oligonucleotide (A9L) with comparable binding affinity and activity to A9 and A9g (Fig. 5C).

The successful truncation of the A9 PSMA aptamer is of importance in the light of recent data directly implicating PSMA's enzymatic activity in promoting carcinogenesis (Lapidus et al., 2000; Yao et al., 2010). PSMA has multiple catalytic activities, including NAALADase, folatecarboxypeptidase, and dipeptidyl peptidase IV activity (Bacich et al., 2001). Recent studies have suggested a role for PSMA enzymatic activity in cell migration and activation of oncogenic pathways (Lapidus et al., 2000; Yao et al., 2010). Importantly, inhibition of PSMA enzymatic activity by small molecule inhibitors abrogates PSMA-mediated carcinogenesis ((Kularatne et al., 2009; Yao et al., 2010) and our unpublished data). Here, we show that the A9g (43 mer) and A9L (41 mer) aptamers, similar to A9, retain the ability to inhibit PSMA's NAALADase activity (Fig. 5C) and, thus, could be employed as therapeutic inhibitors of PSMA. In contrast, a previously described truncated version of the A10 PSMA aptamer (A10-3.2; 39 mer), which retains binding to PSMA (Dassie et al., 2009), is unable to inhibit PSMA NAALADase activity (Fig. 1A).

The A10-3.2 aptamer has been successfully used by us to deliver siRNAs targeting cancer prosurvival genes to PSMA-expressing prostate cancer cells (Dassie et al., 2009). In this context, the truncated aptamer serves solely as a delivery tool for the therapeutic siRNA cargo. In principle, conjugation of therapeutic siRNAs to the A9g and A9L aptamers, which we demonstrate internalize efficiently and specifically into PSMA-expressing cells (Fig. 6), could result in dual function-targeted reagents that are capable of inhibiting multiple carcinogenic pathways (PSMA and prosurvivalgenes). An aptamer-siRNA conjugate with dual function has been previously described for the treatment of HIV infected cells (Zhou et al., 2008). In this article, an inhibitory aptamer against gp120 was tethered to an siRNA against *tat/rev*, 2 viral genes that drive replication of the virus. The aptamer-siRNA combination reduced HIV infectivity and replication in cultured T cells (Zhou et al., 2008) and suppressed HIV-1 viral loads reversing CD4+ T cell decline in a humanized mouse model of HIV (Neff et al., 2011).

In principle, the information provided by the theoretical secondary and tertiary RNA structure models can be used not only to guide in the truncation of long RNA oligonucleotide sequences (as described herein) but also to enable the modification of key nucleotides to improve overall aptamer quality and function (Zhou et al., 2011). Although large-scale, high-quality cGMP-grade (Current Good Manufacturing Process) synthesis of long RNA oligonucleotide aptamers (60–100 nucleotides long) remains a rate limiting step to their therapeutic potential (Reese, 2005), other *in vivo* properties of these RNAs, such as their pharmacokinetics (PK) and pharmacodynamics (PD), can also hinder their therapeutic utility [reviewed in (Keefe et al., 2010)]. Several ways to optimize the PK/PD of aptamers have been described. These include (1) the use of modified nucleotides that impart nuclease resistance, thus resulting in RNA aptamers with longer half lives in the blood (Lin et al., 1994; Ruckman et al., 1998) and (2) chemical conjugation of high-molecular-weight molecules (eg, 20–40 kDa PEG) to prevent exclusion by renal filtration (Kawaguchi et al., 1995; Watson et al., 2000; Healy et al., 2004). Although 2′-fluoro modified pyrimidines are usually incorporated into RNA aptamers during the selection process, additional modifications are introduced postselection, using an atrial-and-error approach that is laborious and is not guaranteed to work for all aptamers (Ruckman et al., 1998; Floege et al., 1999; Adler et al., 2008). In principle, theoretical RNA structure algorithms similar to the ones described herein can be utilized to identify bases that when modified (with synthetic bases) may increase the overall thermodynamic stability and nuclease resistance of these RNA aptamers without loss of function. Likewise, these algorithms can be used to identify critical residues that cannot tolerate modifications (Fig. 5A).

In conclusion, our studies highlight the utility of theoretical RNA secondary and tertiary structure models and protein docking studies for guiding the truncation of RNA aptamers to enable and expedite large-scale chemical synthesis of these RNAs for clinical applications. Importantly, these efforts have resulted in a truncated PSMA A9 aptamer that due to its shorter sequence length is now amenable to large-scale chemical synthesis for targeted therapeutic applications in the setting of prostate cancer. Finally, the ability to directly test the computer-generated structural predictions by using robust functional assays (binding and enzymatic activity) can enable the refinement of current RNA prediction algorithms. Once refined, these theoretical models can be applied to optimize other aptamers with therapeutic potential.

Acknowledgments

The authors thank Dr. Luiza Hernandez for careful editing of this article. This work was supported by funding from the National Institutes of Health [1RO1 CA138503-01 and 1R21DE019953-01 to PHG; GM063732 to SJC; R21GM088517 to XQ]; the National Science Foundation [MCB0920411, MCB0920067 to SJC; NSF CAREER Award DBI-0953839 to XZ]; the Roy J. Carver Charitable Trust [RJCCT 01-224 to PHG]; and the RSNA Research Resident Grant [RR0905 to WMR].

Disclosure Statement

No competing financial interests exist.

References

ADLER, A., FORSTER, N., HOMANN, M., and GORINGER, H.U. (2008). Post-SELEX chemical optimization of a trypanosome-specific RNA aptamer. Comb. Chem. High Throughput Screen. **11,** 16–23.

ARRAIANO, C.M., BARBAS, A., and AMBLAR, M. (2008). Characterizing ribonucleases *in vitro* examples of synergies between biochemical and structural analysis. Methods Enzymol. **447,** 131–160.

BACICH, D.J., PINTO, J.T., TONG, W.P., and HESTON, W.D. (2001). Cloning, expression, genomic localization, and enzymatic activities of the mouse homolog of prostate-specific membrane antigen/NAALADase/folate hydrolase. Mamm. Genome **12,** 117–123.

BAGALKOT, V., FAROKHZAD, O.C., LANGER, R., and JON, S. (2006). An aptamer-doxorubicin physical conjugate as a novel targeted drug-delivery platform. Angew. Chem. Int. Ed. Engl. **45,** 8149–8152.

BIESECKER, G., DIHEL, L., ENNEY, K., and BENDELE, R.A. (1999). Derivation of RNA aptamer inhibitors of human complement C5. Immunopharmacology **42,** 219–230.

BUFF, M.C., SCHAFER, F., WULFFEN, B., MULLER, J., POTZSCH, B., HECKEL, A., and MAYER, G. (2010). Dependence of aptamer activity on opposed terminal extensions: improvement of light-regulation efficiency. Nucleic Acids Res. **38,** 2111–2118.

BURGSTALLER, P., KOCHOYAN, M., and FAMULOK, M. (1995). Structural probing and damage selection of citrulline- and arginine-specific RNA aptamers identify base positions required for binding. Nucleic Acids Res. **23,** 4769–4776.

BURMEISTER, P.E., LEWIS, S.D., SILVA, R.F., PREISS, J.R., HORWITZ, L.R., PENDERGRAST, P.S., MCCAULEY, T.G., KURZ, J.C., EPSTEIN, D.M., WILSON, C., and KEEFE, A.D. (2005). Direct *in vitro* selection of a 2′-O-methyl aptamer to VEGF. Chem. Biol. **12,** 25–33.

BURMEISTER, P.E., WANG, C., KILLOUGH, J.R., LEWIS, S.D., HORWITZ, L.R., FERGUSON, A., THOMPSON, K.M., PENDERGRAST, P.S., MCCAULEY, T.G., KURZ, M., DIENER, J., CLOAD, S.T., WILSON, C., and KEEFE, A.D. (2006). 2′-Deoxy purine, 2′-O-methyl pyrimidine (dRmY) aptamers as candidate therapeutics. Oligonucleotides **16,** 337–351.

CAO, S., and CHEN, S.J. (2005). Predicting RNA folding thermodynamics with a reduced chain representation model. RNA **11,** 1884–1897.

CAO, S., and CHEN, S.J. (2006). Free energy landscapes of RNA/RNA complexes: with applications to snRNA complexes in spliceosomes. J. Mol. Biol. **357,** 292–312.

CAO, S., and CHEN, S.J. (2009). A new computational approach for mechanical folding kinetics of RNA hairpins. Biophys. J. **96,** 4024–4034.

CAO, S., and CHEN, S.J. (2011). Physics-based de novo prediction of RNA 3D structures. J. Phys. Chem. B **115,** 4216–4226.

CAO, S., FURTIG, B., SCHWALBE, H., and CHEN, S.J. (2010). Folding kinetics for the conformational switch between alternative RNA structures. J. Phys. Chem. B **114,** 13609–13615.

CAO, Z., TONG, R., MISHRA, A., XU, W., WONG, G.C., CHENG, J., and LU, Y. (2009). Reversible cell-specific drug delivery with aptamer-functionalized liposomes. Angew. Chem. Int. Ed. Engl. **48,** 6494–6498.

CASE, D.A., CHEATHAM, T.E., 3rd, DARDEN, T., GOHLKE, H., LUO, R., MERZ, K.M., JR., ONUFRIEV, A., SIMMERLING, C., WANG, B., and WOODS, R.J. (2005). The Amber biomolecular simulation programs. J. Comput. Chem. **26,** 1668–1688.

CHAKRAVARTHY, U., ADAMIS, A.P., CUNNINGHAM, E.T., JR., GOLDBAUM, M., GUYER, D.R., KATZ, B., and PATEL, M. (2006). Year 2 efficacy results of 2 randomized controlled clinical trials of pegaptanib for neovascular age-related macular degeneration. Ophthalmology **113,** 1508, e1501–e1525.

CHEN, S.J. (2008). RNA folding: conformational statistics, folding kinetics, and ion electrostatics. Annu. Rev. Biophys. **37,** 197–214.

CHU, T.C., TWU, K.Y., ELLINGTON, A.D., and LEVY, M. (2006). Aptamer mediated siRNA delivery. Nucleic Acids Res. **34,** e73.

COLOMBATTI, M., GRASSO, S., PORZIA, A., FRACASSO, G., SCUPOLI, M.T., CINGARLINI, S., POFFE, O., NAIM, H.Y., HEINE, M., TRIDENTE, G., MAINIERO, F., and RAMARLI, D. (2009). The prostate specific membrane antigen regulates the expression of IL-6 and CCL5 in prostate tumour cells by activating the MAPK pathways. PLoS One **4,** e4608.

COSMI, B. (2009). ARC-1779, a PEGylated aptamer antagonist of von Willebrand factor for potential use as an anticoagulant or antithrombotic agent. Curr. Opin. Mol. Ther. **11,** 322–328.

DARTY, K., DENISE, A., and PONTY, Y. (2009). VARNA: interactive drawing and editing of the RNA secondary structure. Bioinformatics **25,** 1974–1975.

DASSIE, J.P., LIU, X.Y., THOMAS, G.S., WHITAKER, R.M., THIEL, K.W., STOCKDALE, K.R., MEYERHOLZ, D.K., MCCAFFREY, A.P., MCNAMARA, J.O., 2nd, and GIANGRANDE, P.H. (2009). Systemic administration of optimized aptamer-siRNA chimeras promotes regression of PSMA-expressing tumors. Nat. Biotechnol. **27,** 839–849.

DAVIS, M.I., BENNETT, M.J., THOMAS, L.M., and BJORKMAN, P.J. (2005). Crystal structure of prostate-specific membrane antigen, a tumor marker and peptidase. Proc. Natl. Acad. Sci. U. S. A. **102,** 5981–5986.

DHAR, S., GU, F.X., LANGER, R., FAROKHZAD, O.C., and LIPPARD, S.J. (2008). Targeted delivery of cisplatin to prostate cancer cells by aptamer functionalized Pt(IV) prodrug-PLGA-PEG nanoparticles. Proc. Natl. Acad. Sci. U. S. A. **105,** 17356–17361.

DHAR, S., KOLISHETTI, N., LIPPARD, S.J., and FAROKHZAD, O.C. (2011). Targeted delivery of a cisplatin prodrug for safer and more effective prostate cancer therapy *in vivo*. Proc. Natl. Acad. Sci. U. S. A. **108,** 1850–1855.

DYKE, C.K., STEINHUBL, S.R., KLEIMAN, N.S., CANNON, R.O., ABERLE, L.G., LIN, M., MYLES, S.K., MELLONI, C., HARRINGTON, R.A., ALEXANDER, J.H., BECKER, R.C., and RUSCONI, C.P. (2006). First-in-human experience of an antidote-controlled anticoagulant using RNA aptamer technology: a phase 1a pharmacodynamic evaluation of a drug-antidote pair for the controlled regulation of factor IXa activity. Circulation **114,** 2490–2497.

EIKELBOOM, J.W., ZELENKOFSKE, S.L., and RUSCONI, C.P. (2010). Coagulation factor IXa as a target for treatment and prophylaxis of venous thromboembolism. Arterioscler. Thromb. Vasc. Biol. **30,** 382–387.

ELLINGTON, A.D., and SZOSTAK, J.W. (1990). *In vitro* selection of RNA molecules that bind specific ligands. Nature **346,** 818–822.

FAROKHZAD, O.C., JON, S., KHADEMHOSSEINI, A., TRAN, T.N., LAVAN, D.A., and LANGER, R. (2004). Nanoparticle-aptamer bioconjugates: a new approach for targeting prostate cancer cells. Cancer Res. **64,** 7668–7672.

FLOEGE, J., OSTENDORF, T., JANSSEN, U., BURG, M., RADEKE, H.H., VARGEESE, C., GILL, S.C., GREEN, L.S., and JANJIC, N. (1999). Novel approach to specific growth factor inhibition *in vivo*: antagonism of platelet-derived growth factor in glomerulonephritis by aptamers. Am. J. Pathol. **154,** 169–179.

GILBERT, J.C., DEFEO-FRAULINI, T., HUTABARAT, R.M., HORVATH, C.J., MERLINO, P.G., MARSH, H.N., HEALY, J.M., BOUFAKHREDDINE, S., HOLOHAN, T.V., and SCHAUB, R.G. (2007). First-in-human evaluation of anti von Willebrand factor therapeutic aptamer ARC1779 in healthy volunteers. Circulation **116,** 2678–2686.

GRAGOUDAS, E.S., ADAMIS, A.P., CUNNINGHAM, E.T., JR., FEINSOD, M., and GUYER, D.R. (2004). Pegaptanib for neovascular age-related macular degeneration. N. Engl. J. Med. **351,** 2805–2816.

GREEN, L., WAUGH, S., BINKLEY, J.P., HOSTOMSKA, Z., HOSTOMSKY, Z., and TUERK, C. (1995). Comprehensive chemical modification interference and nucleotide substitution analysis of an RNA pseudoknot inhibitor to HIV-1 reverse transcriptase. J. Mol. Biol. **247,** 60–68.

GU, F., ZHANG, L., TEPLY, B.A., MANN, N., WANG, A., RADOVIC-MORENO, A.F., LANGER, R., and FAROKHZAD, O.C. (2008). Precise engineering of targeted nanoparticles by using self-assembled biointegrated block copolymers. Proc. Natl. Acad. Sci. U. S. A. **105,** 2586–2591.

HEALY, J.M., LEWIS, S.D., KURZ, M., BOOMER, R.M., THOMPSON, K.M., WILSON, C., and MCCAULEY, T.G. (2004). Pharmacokinetics and biodistribution of novel aptamer compositions. Pharm. Res. **21,** 2234–2246.

HERNANDEZ, F.J., KALRA, N., WENGEL, J., and VESTER, B. (2009). Aptamers as a model for functional evaluation of LNA and 2′-amino LNA. Bioorg. Med. Chem. Lett. **19,** 6585–6587.

HICKE, B.J., STEPHENS, A.W., GOULD, T., CHANG, Y.F., LYNOTT, C.K., HEIL, J., BORKOWSKI, S., HILGER, C.S., COOK, G., WARREN, S., and SCHMIDT, P.G. (2006). Tumor targeting by an aptamer. J. Nucl. Med. **47,** 668–678.

HUANG, Y., ECKSTEIN, F., PADILLA, R., and SOUSA, R. (1997). Mechanism of ribose 2′-group discrimination by an RNA polymerase. Biochemistry **36,** 8231–8242.

HUANG, S.Y., and ZOU, X. (2008). An iterative knowledge-based scoring function for protein-protein recognition. Proteins **72,** 557–579.

HUANG, S.Y., and ZOU, X. (2010). MDockPP: A hierarchical approach for protein-protein docking and its application to CAPRI rounds 15–19. Proteins **78,** 3096–3103.

JELLINEK, D., GREEN, L.S., BELL, C., LYNOTT, C.K., GILL, N., VARGEESE, C., KIRSCHENHEUTER, G., MCGEE, D.P., ABESINGHE, P., PIEKEN, W.A., et al. (1995). Potent 2′-amino-2′-deoxypyrimidine RNA inhibitors of basic fibroblast growth factor. Biochemistry **34,** 11363–11372.

KATILIUS, E., FLORES, C., and WOODBURY, N.W. (2007). Exploring the sequence space of a DNA aptamer using microarrays. Nucleic Acids Res. **35,** 7626–7635.

KAWAGUCHI, T., ASAKAWA, H., TASHIRO, Y., JUNI, K., and SUEISHI, T. (1995). Stability, specific binding activity, and plasma concentration in mice of an oligodeoxynucleotide modified at 5′-terminal with poly(ethylene glycol). Biol. Pharm. Bull. **18,** 474–476.

KEEFE, A.D., PAI, S., and ELLINGTON, A. (2010). Aptamers as therapeutics. Nat. Rev. Drug Discov. **9,** 537–550.

KULARATNE, S.A., WANG, K., SANTHAPURAM, H.K., and LOW, P.S. (2009). Prostate-specific membrane antigen targeted imaging and therapy of prostate cancer using a PSMA inhibitor as a homing ligand. Mol. Pharm. **6,** 780–789.

LAPIDUS, R.G., TIFFANY, C.W., ISAACS, J.T., and SLUSHER, B.S. (2000). Prostate-specific membrane antigen (PSMA) enzyme activity is elevated in prostate cancer cells. Prostate **45,** 350–354.

LIN, Y., QIU, Q., GILL, S.C., and JAYASENA, S.D. (1994). Modified RNA sequence pools for *in vitro* selection. Nucleic Acids Res. **22,** 5229–5234.

LUPOLD, S.E., HICKE, B.J., LIN, Y., and COFFEY, D.S. (2002). Identification and characterization of nuclease-stabilized RNA molecules that bind human prostate cancer cells via the prostate-specific membrane antigen. Cancer Res. **62,** 4029–4033.

MATHEWS, D.H. (2006). RNA secondary structure analysis using RNA structure. Curr. Protoc. Bioinform. **Chapter 12,** Unit 12.6.

MATHEWS, D.H., TURNER, D.H., and ZUKER, M. (2007). RNA secondary structure prediction. Curr. Protoc. Nucleic Acid Chem. **Chapter 11,** Unit 11.2.

MCNAMARA, J.O., 2nd, ANDRECHEK, E.R., WANG, Y., VILES, K.D., REMPEL, R.E., GILBOA, E., SULLENGER, B.A., and GIANGRANDE, P.H. (2006). Cell type-specific delivery of siRNAs with aptamer-siRNA chimeras. Nat. Biotechnol. **24,** 1005–1015.

MCNAMARA, J.O., KOLONIAS, D., PASTOR, F., MITTLER, R.S., CHEN, L., GIANGRANDE, P.H., SULLENGER, B., and GILBOA, E. (2008). Multivalent 4-1BB binding aptamers costimulate CD8+ T cells and inhibit tumor growth in mice. J. Clin. Invest. **118,** 376–386.

MONGELARD, F., and BOUVET, P. (2010). AS-1411, a guanosine-rich oligonucleotide aptamer targeting nucleolin for the potential treatment of cancer, including acute myeloid leukemia. Curr. Opin. Mol. Ther. **12,** 107–114.

NEFF, C.P., ZHOU, J., REMLING, L., KURUVILLA, J., ZHANG, J., LI, H., SMITH, D.D., SWIDERSKI, P., ROSSI, J.J., and AKKINA, R. (2011). An aptamer-siRNA chimera suppresses HIV-1 viral loads and protects from helper CD4(+) T cell decline in humanized mice. Sci. Transl. Med. **3,** 66ra6.

NG, E.W., and ADAMIS, A.P. (2006). Anti-VEGF aptamer (pegaptanib) therapy for ocular vascular diseases. Ann. N.Y. Acad. Sci. **1082,** 151–171.

PADILLA, R., and SOUSA, R. (1999). Efficient synthesis of nucleic acids heavily modified with non-canonical ribose 2′-groups using a mutantT7 RNA polymerase (RNAP). Nucleic Acids Res. **27,** 1561–1563.

PASTOR, F., KOLONIAS, D., GIANGRANDE, P.H., and GILBOA, E. (2010). Induction of tumour immunity by targeted inhibition of nonsense-mediated mRNA decay. Nature **465,** 227–230.

REESE, C.B. (2005). Oligo- and poly-nucleotides: 50 years of chemical synthesis. Org. Biomol. Chem. **3,** 3851–3868.

RUCKMAN, J., GREEN, L.S., BEESON, J., WAUGH, S., GILLETTE, W.L., HENNINGER, D.D., CLAESSON-WELSH, L., and JANJIC, N. (1998). 2′-Fluoropyrimidine RNA-based aptamers to the 165-amino acid form of vascular endothelial growth factor (VEGF165). Inhibition of receptor binding and VEGF-induced vascular permeability through interactions requiring the exon 7-encoded domain. J. Biol. Chem. **273,** 20556–20567.

RUSCONI, C.P., SCARDINO, E., LAYZER, J., PITOC, G.A., ORTEL, T.L., MONROE, D., and SULLENGER, B.A. (2002). RNA aptamers as reversible antagonists of coagulation factor IXa. Nature **419,** 90–94.

SASSANFAR, M., and SZOSTAK, J.W. (1993). An RNA motif that binds ATP. Nature **364,** 550–553.

SERRA, M.J., and TURNER, D.H. (1995). Predicting thermodynamic properties of RNA. Methods Enzymol. **259,** 242–261.

SILVER, D.A., PELLICER, I., FAIR, W.R., HESTON, W.D., and CORDON-CARDO, C. (1997). Prostate-specific membrane antigen expression in normal and malignant human tissues. Clin. Cancer Res. **3,** 81–85.

SOONTORNWORAJIT, B., ZHOU, J., SNIPES, M.P., BATTIG, M.R., and WANG, Y. (2011). Affinity hydrogels for controlled protein release using nucleic acid aptamers and complementary oligonucleotides. Biomaterials **32,** 6839–6849.

THIEL, K.W., and GIANGRANDE, P.H. (2009). Therapeutic applications of DNA and RNA aptamers. Oligonucleotides **19,** 209–222.

WATSON, S.R., CHANG, Y.F., O'CONNELL, D., WEIGAND, L., RINGQUIST, S., and PARMA, D.H. (2000). Anti-L-selectin aptamers: binding characteristics, pharmacokinetic parameters, and activity against an intravascular target *in vivo*. Antisense Nucleic Acid Drug Dev. **10,** 63–75.

WONG, I., and LOHMAN, T.M. (1993). A double-filter method for nitrocellulose-filter binding: application to protein-nucleic acid interactions. Proc. Natl. Acad. Sci. U. S. A. **90,** 5428–5432.

XIAO, Z., JIANG, X., BECKETT, M.L., and WRIGHT, G.L., JR. (2000). Generation of a baculovirus recombinant prostate-specific membrane antigen and its use in the development of a novel protein biochip quantitative immunoassay. Protein Expr. Purif. **19,** 12–21.

YAO, V., BERKMAN, C.E., CHOI, J.K., O'KEEFE, D.S., and BACICH, D.J. (2010). Expression of prostate-specific membrane antigen (PSMA), increases cell folate uptake and proliferation and suggests a novel role for PSMA in the uptake of the non-polyglutamated folate, folic acid. Prostate **70,** 305–316.

ZHOU, J., LI, H., LI, S., ZAIA, J., and ROSSI, J.J. (2008). Novel dual inhibitory function aptamer-siRNA delivery system for HIV-1 therapy. Mol. Ther. **16,** 1481–1489.

ZHOU, J., SOONTORNWORAJIT, B., SNIPES, M.P., and WANG, Y. (2011). Structural prediction and binding analysis of hybridized aptamers. J. Mol. Recognit. **24,** 119–126.

ZHOU, J., SWIDERSKI, P., LI, H., ZHANG, J., NEFF, C.P., AKKINA, R., and ROSSI, J.J. (2009). Selection, characterization and application of new RNA HIV gp 120 aptamers for facile delivery of Dicer substrate siRNAs into HIV infected cells. Nucleic Acids Res. **37,** 3094–3109.

Address correspondence to:
Dr. Paloma H. Giangrande
Department of Internal Medicine
University of Iowa
285 Newton Road
5202 MERF
Iowa City, IA 52242

E-mail: paloma-giangrande@uiowa.edu

Received for publication July 7, 2011; accepted after revision August 18, 2011.